SPECIAL
ISARS 2012
COLLECTION

Model of the Correlation between Lidar Systems and Wind Turbines for Lidar-Assisted Control

DAVID SCHLIPF AND PO WEN CHENG

Stuttgart Wind Energy, Universität Stuttgart, Stuttgart, Germany

JAKOB MANN

DTU Wind Energy, Technical University of Denmark, Risø Campus, Denmark

ABSTRACT

Investigations of lidar-assisted control to optimize the energy yield and to reduce loads of wind turbines have increased significantly in recent years. For this kind of control, it is crucial to know the correlation between the rotor effective wind speed and the wind preview provided by a nacelle- or spinner-based lidar system. If on the one hand, the assumed correlation is overestimated, then the uncorrelated frequencies of the preview will cause unnecessary control action, inducing undesired loads. On the other hand, the benefits of the lidar-assisted controller will not be fully exhausted, if correlated frequencies are filtered out. To avoid these miscalculations, this work presents a method to model the correlation between lidar systems and wind turbines using Kaimal wind spectra. The derived model accounts for different measurement configurations and spatial averaging of the lidar system, different rotor sizes, and wind evolution. The method is compared to real measurement data with promising results. In addition, examples depict how this model can be used to design an optimal controller and how the configuration of a lidar system is optimized for a given turbine to improve the correlation.

1. Introduction

Lidar systems are able to provide information about the wind field approaching a wind turbine in advance, which can be used to assist wind turbine control. This field of investigations has increased significantly in recent years, and several controllers for load reduction or energy yield increase have been tested in simulations (see, e.g., Laks et al. 2010; Dunne et al. 2012; Schlipf et al. 2013b; Koerber and King 2011; Henriksen 2011; Kragh et al. 2013). The latest work also considers wind evolution (see Bossanyi 2012; Simley et al. 2012; Laks et al. 2013).

Initial field testing of lidar-assisted feedforward collective pitch control shows that improvement of the control performance can be confirmed in reality and proves that the performance of lidar-assisted control is

dependent on the correlation between the lidar system and the turbine (see Schlipf et al. 2012a; Scholbrock et al. 2013).

In this work, a new analytic model of correlation between the rotor effective wind speed of the turbine and the lidar estimate is derived based on models of turbulent wind, lidar measurement, and wind evolution. Previous work is based on simulated or real measurements to the knowledge of the authors (see Schlipf et al. 2010a; Simley et al. 2013). Here, techniques from signal processing are used to build up a modular and extensible framework. This model can be used in the planning of a lidar-assisted control project to determine whether a lidar system is able to provide useful signals or to optimize the configuration or scanning pattern of a lidar system. Furthermore, the model was used successfully in field testing to evaluate the lidar measurements and to design an adaptive filter, the core of the used controller.

This paper is organized as follows. In section 2 the requirements for the feedforward collective pitch control

Corresponding author address: David Schlipf, SWE, Universität Stuttgart, Allmandring 5B, 70569 Stuttgart, Germany.
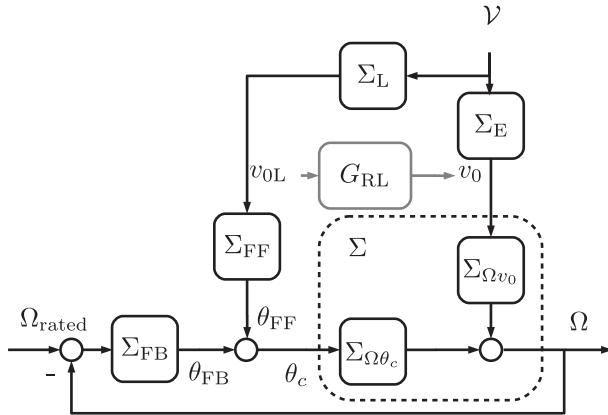E-mail: schlipf@ifb.uni-stuttgart.de

FIG. 1. The Σ_{FF} tries to compensate the effects of $\mathcal{V}$ to Ω of Σ by adding a pitch update to Σ_{FB}. The Σ_E and Σ_L are modeled by G_{RL}, which can be used as an optimal filter.

are explained. In sections 3 and 4, the model for a perfect staring and a real scanning lidar is derived, which is evaluated with data from the field testing in section 5. The model is used in section 6 to optimize a lidar system, and conclusions and future work are discussed in section 7.

2. Requirements for control

Reducing fatigue and extreme loads of the structure is an important design goal for the control of large wind turbines. Transient events such as gusts represent an unknown disturbance to the control system. Conventional feedback controllers can only provide delayed compensation for such excitations, since the disturbance effects must propagate through the entire wind turbine before showing its effects in the measured outputs. This usually results in additional loads for the wind turbine and requires high actuator rates for the disturbance compensation. These effects can be avoided if the wind ahead of the wind turbine is measured by remote sensing techniques such as lidar and the information is fed to the turbine controller.

The magnitude of load reduction depends on the quality of the wind preview, expressed by the correlation of the lidar measurements and the turbine reaction. In this section the requirements of the correlation for lidar-assisted control are derived by a description of a feedforward collective pitch controller. The same approach can be used for the direct speed controller to optimize the energy yield (see Schlipf et al. 2013a).

The feedforward controller (see Fig. 1) is based on the work in Schlipf et al. (2010a) and combines the baseline feedback controller with a feedforward update. The main control goal of the collective pitch feedback controller

Σ_{FB} is to maintain the rated rotor speed Ω_{rated}. The system Σ is disturbed by a wind field $\mathcal{V}$, which can be measured by a lidar system Σ_L in front of the turbine before reaching the rotor. If the wind does not change on its way ($\Sigma_E = 1$), then in the case of perfect measurement the measured wind speed v_{0L} and the rotor effective wind speed v_0 are equal. The disturbance could be perfectly compensated by a feedforward controller $\Sigma_{FF} = -\Sigma_{\Omega\theta_c}^{-1}\Sigma_{\Omega v_0}$, if the influence on the rotor speed of the wind $\Sigma_{\Omega v_0}$ and the pitch angle $\Sigma_{\Omega\theta_c}$ is known and $\Sigma_{\Omega\theta_c}$ is invertible.

In reality v_0 cannot be measured perfectly because of the wind evolution Σ_E and the limitation of the lidar system Σ_L. Therefore, the needed feedforward controller is

$$\Sigma_{FF} = -\Sigma_{\Omega\theta_c}^{-1}\Sigma_{\Omega v_0}\Sigma_E\Sigma_L^{-1}. \tag{1}$$

Because of the interaction with the turbine and missing technology, modeling and verifying Σ_E is very complicated. Also, not all information of V be reconstructed by the inverse of Σ_L. However, if the transfer function G_{RL} from the measured wind speed to the rotor effective wind speed is known, then it can be used to exploit all information captured by the lidar system:

$$\Sigma_{FF} = -\Sigma_{\Omega\theta_c}^{-1}\Sigma_{\Omega v_0}G_{RL}. \tag{2}$$

For real-time applications, G_{RL} can be obtained from measurements and approximated by a standard low-pass filter. Therefore, the cutoff frequency (-3 dB) of the corresponding filter can be considered as a quality criterion for the correlation. In the following sections, an analytic way to estimate both the transfer function

$$G_{RL} = \frac{S_{RL}}{S_{LL}} \tag{3}$$

and the squared coherence

$$\gamma_{RL}^2 = \frac{|S_{RL}|^2}{S_{RR}S_{LL}} \tag{4}$$

is presented using the autospectrum S_{LL} from the lidar and S_{RR} from the rotor, as well as the cross-spectrum S_{RL} between the rotor and the lidar.

3. Correlation of a perfect staring lidar system

The calculation of S_{LL}, S_{RR}, and S_{RL} for a perfect staring lidar system is done fully and semianalytically. They are derived based on Kaimal wind spectra, but in

principle other wind spectra models can be used. The spectra $S_{ii,h}$ of the longitudinal ($h = 1$), lateral ($h = 2$), and upward ($h = 3$) velocity component in point i is given in the International Electrotechnical Commission (IEC) standard 61400-1 (IEC 2005) by the equation:

$$\frac{fS_{ii,h}}{\sigma_h^2} = \frac{4fL_h/\overline{u}}{(1 + 6fL_h/\overline{u})^{5/3}}, \tag{5}$$

where f is the frequency; σ_h and L_h are the standard deviation and the integral-scale parameter of the corresponding velocity component, respectively; and $\overline{u}$ is the mean of the longitudinal velocity component at hub height. The coherence of the longitudinal velocity component between two points in the rotor plane with distance r_{ij} is defined as

$$\gamma_{ij,1} = \frac{S_{ij,1}}{S_{ii,1}} = \exp\left(-12\sqrt{(f/\overline{u})^2 + (0.12/L_1)^2}\, r_{ij}\right)$$
$$= \exp(-\kappa r_{ij}), \tag{6}$$

where κ is the frequency-dependent lateral decay parameter and $S_{ij,1}$ is the cross-spectrum between points i and j, and assuming that the rotor plane is normal to the average wind direction.

Ignoring the filtering effect of a lidar and assuming Taylor's frozen turbulence hypothesis (Taylor 1938) to be fully valid (no wind evolution), the lidar estimate of the rotor effective wind speed can be considered equal to the longitudinal wind velocity u_{HH} at the hub:

$$v_{0L} = u_{HH}. \tag{7}$$

Therefore, the spectrum of a staring lidar system can be modeled with the spectrum at the hub (5) by

$$S_{LL} = S_{HH,1}. \tag{8}$$

The rotor-averaged spectrum can be derived by an average of the cross- and autospectrum densities of all points and combinations in the rotor plane A with rotor radius R:

$$S_{RR} = \frac{1}{(\pi R^2)^2} \int_{A_j} \int_{A_i} S_{ij,1}\, dy_i\, dz_i\, dy_j\, dz_j. \tag{9}$$

The origin of the orthonormal coordinate system used in this work is the rotor hub, and the x, y, and z axes are pointing in the downwind, lateral, and upward directions, respectively. With (6) the explicit solution of (9) can be found as

$$S_{RR} = \frac{2S_{HH,1}}{3\pi(R\kappa)^3}\{R\kappa[-9\pi_0\tilde{F}_1(;2;(R\kappa)^2) - 6\pi\mathbf{L}_2(2R\kappa)$$
$$- 8R\kappa + 6\pi I_0(2R\kappa) + 3\pi] + 3\pi\mathbf{L}_1(2R\kappa)\}, \tag{10}$$

where $_0\tilde{F}_1$ is the regularized confluent hypergeometric function, $\mathbf{L}_n$ is the modified Struve function, and I_0 is the modified Bessel function of the first kind. Furthermore, it is assumed that the autospectra of the three wind components in all points are equal to the spectra $S_{HH,h}$ at the hub.

Similar to (9), the cross-spectrum between the staring lidar system and the rotor is

$$S_{RL} = \frac{1}{\pi R^2} \int_A S_{Hj,1}\, dy_j\, dz_j. \tag{11}$$

With $S_{Hj,1}$ and $\gamma_{Hj,1}$ as the cross-spectrum and coherence of the longitudinal wind component between the hub and the point j, respectively, (11) is solved by

$$S_{RL} = \frac{S_{HH,1}}{\pi R^2} \int_0^{2\pi} \int_0^R r\gamma_{Hj,1}\, dr\, d\phi = \frac{2S_{HH,1}}{R^2\kappa^2}\left[1 - \frac{R\kappa + 1}{\exp(R\kappa)}\right]. \tag{12}$$

With (3), (4), and

$$k = \frac{2\pi f}{\overline{u}}, \tag{13}$$

G_{RL} and the squared coherence γ_{RL}^2 can be calculated over the wavenumber k, independent of the mean wind speed $\overline{u}$.

Furthermore, a semianalytic approach is developed to avoid the integration necessary for the derivation of the correlation model. Therefore, the rotor effective wind speed is considered to be equal to the mean of all n longitudinal wind components u_i hitting the rotor plane:

$$v_0 = \frac{1}{n} \sum_{i=1}^n u_i. \tag{14}$$

A weighting function considering tip and root losses (see Schlipf and Kühn 2008) could improve the results, but it would increase the complexity of the model. With the definition of Bendat and Piersol (1971), cross- and autospectra can be calculated, omitting all scaling constants, by

$$S_{RR} = \overline{\mathcal{F}\{v_0\}\mathcal{F}^*\{v_0\}},$$
$$S_{RL} = \overline{\mathcal{F}\{v_0\}\mathcal{F}^*\{v_{0L}\}}, \quad \text{and}$$
$$S_{LL} = \overline{\mathcal{F}\{v_{0L}\}\mathcal{F}^*\{v_{0L}\}}, \tag{15}$$

where $\mathcal{F}\{\cdot\}$ and $\mathcal{F}^*\{\cdot\}$ are the Fourier transform and its complex conjugate, respectively. For the perfect staring lidar system, this yields

$$S_{RR} = \frac{S_{HH,1}}{n^2} \sum_{i=1}^{n} \sum_{j=1}^{n} \gamma_{ij,1} \quad \text{and}$$

$$S_{RL} = \frac{S_{HH,1}}{n} \sum_{j=1}^{n} \gamma_{Hj,1}. \tag{16}$$

With (16) G_{RL} and γ_{RL}^2 can be calculated in a straightforward manner, and the differences compared to using (10) and (12) are decreasing with increasing n.

4. Correlation of a real scanning lidar system

For a real scanning lidar system, the following effects are integrated into the semianalytic model: discrete scanning, wind evolution, spatial averaging, and wind reconstruction. These effects will make the calculation of v_{0L} more complex, but the main idea of the approach can still be used: The measured wind can be considered as a sum of signals and because of the linearity of the Fourier transformation, the spectra can be calculated by a sum of auto- and cross-spectra.

All effects except wind evolution are verified isolated and in combination with a lidar simulator from Schlipf et al. (2009) and a TurbSim wind field simulator (Jonkman and Buhl 2007). The model agrees with the correlation of the rotor effective wind speed from the simulated lidar and the wind field, if the wind field is only evaluated at the grid points, because interpolation in the grid overestimates the correlation.

In the following subsections the effects will be explained separately, giving a simple example. The spectrum of a real scanning lidar system is a combination of all these effects.

a. Discrete scanning

Real lidar systems with only one laser source measuring in different points have to scan sequentially. But also lidar systems with one laser source for each point need to measure for a certain time. This can be modeled by a running average. For example, the measurement of a staring lidar system with measurement time T is represented by

$$v_{0L} = \sum_{m=-\infty}^{\infty} u_{HH}(t) \text{rect}\left(\frac{t - T/2 - mT}{T}\right)$$

$$= u_{HH}(t) * \text{rect}\left(\frac{t - T/2}{T}\right), \tag{17}$$

where $\text{rect}(\cdot)$ is the rectangular function and * denotes convolution, which is translated by the Fourier

transformation as a multiplication of the individual Fourier transforms. Therefore, the resulting autospectrum is

$$S_{LL} = \overline{\mathcal{F}\{v_{0L}\}\mathcal{F}^*\{v_{0L}\}} = \text{sinc}^2(fT) S_{HH,1}, \tag{18}$$

where $\text{sinc}(\cdot)$ is the normalized sinc function used in signal processing.

b. Wind evolution

Wind evolution is here considered by a simple exponential model of coherence, as suggested by Pielke and Panofsky (1970) and Simley et al. (2012). The squared coherence between two points with the longitudinal separation d_{ij} is given by

$$\gamma_{ij,1e}^2 = \exp(-\alpha k d_{ij}), \tag{19}$$

where α is the dimensionless longitudinal decay parameter. Other models such as Kristensen (1979) can also be used. If, for example, a second point downwind is added to the perfect staring lidar system (7), then the rotor effective wind speed estimate can be calculated by shifting the measurement downwind in time considering Taylor's frozen turbulence hypothesis:

$$v_{0L} = \frac{1}{2}[u_1(t) + u_2(t - d_{12}/\overline{u})]. \tag{20}$$

Because of the wind evolution, the resulting spectrum is

$$S_{LL} = \frac{1}{4} S_{HH,1}(2 + 2\gamma_{12,1e}). \tag{21}$$

c. Wind reconstruction

Because of the effect of wind reconstruction as proposed in Schlipf et al. (2011), Kapp and Kühn (2012), and Schlipf et al. (2012b), the lateral and upward wind components distort the lidar estimate of the rotor effective wind speed. The measurement of a lidar system at the point i can be modeled as

$$v_{los,i} = l_{xi}u_i + l_{yi}v_i + l_{zi}w_i, \tag{22}$$

where $[l_{xi}, l_{yi}, l_{zi}]$ is the normalized backscattered laser beam vector and $[u_i, v_i, w_i]$ is the wind vector. If the lidar is perfectly aligned with the wind, then the estimated lateral and vertical wind components are assumed to be zero, and the reconstructed longitudinal component $\hat{u}_i$ can be calculated as

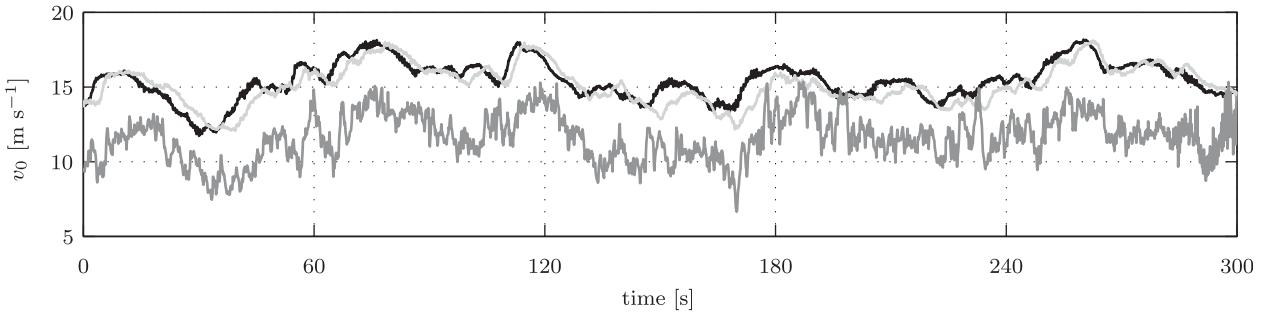$$\hat{u}_i = v_{los,i}/l_{xi}. \tag{23}$$

FIG. 2. Wind speed from the nacelle anemometer (dark gray) and rotor effective wind speed estimates from the CART2 (light gray) and the scanning lidar system (black).

Considering, for example, a lidar system measuring simultaneously in two horizontal points ($l_{zi} = 0$), the rotor effective wind speed is

$$v_{0L} = \frac{1}{2}(\hat{u}_1 + \hat{u}_2) = \frac{1}{2}\left(u_1 + \frac{l_{y1}}{l_{x1}}v_1 + u_2 + \frac{l_{y2}}{l_{x2}}v_2 \right). \quad (24)$$

The resulting spectrum is

$$S_{LL} = \frac{1}{4}\left[S_{HH,1}(2 + 2\gamma_{12,1}) + S_{HH,2}\left(\frac{l_{y1}^2}{l_{x1}^2} + \frac{l_{y2}^2}{l_{x2}^2} \right) \right]. \quad (25)$$

d. Spatial averaging

Because of the pulse length (for pulsed systems) or the optical focusing (for continuous wave systems) and the data processing, real lidar systems average the wind speeds along the laser beam according to a weighting function f_L (see Lindelöw 2008). For pulsed systems it can be assumed that f_L depends only on the distance a to the focus point. For continuous wave systems, there is an additional dependency on the distance to the lidar. With the weighting function $f_L(a)$, it is possible to calculate the line-of-sight wind speed of each focus point i by

$$v_{los,i} = \int_{-\infty}^{\infty} [l_{xi}u_i(a) + l_{yi}v_i(a) + l_{zi}w_i(a)]f_L(a)\, da. \quad (26)$$

Similar to (18) the spectrum could be calculated analytically by a convolution with the Fourier transform $\mathcal{F}\{f_L\}$ of the weighting function, depending on the wavenumber k. But here a discretized approach is used consistent with the overall semianalytic approach. For this purpose, the weighting function is evaluated at discrete distances and the spatial separations are treated similar to the time delays of a temporal filter.

If, for example, the perfect staring lidar model is extended by a weighting function that is evaluated with f_{L1} and f_{L2} at $a_1 = -a$ and $a_2 = a$, then the measurement can be modeled by

$$v_{0L} = \frac{f_{L1}u(-a) + f_{L2}u(a)}{f_{L1} + f_{L2}}. \quad (27)$$

By treating the spatial shift as a delay in the wavenumber domain similar to a temporal shift, the resulting spectrum is

$$\begin{aligned} S_{LL} = \frac{S_{HH,1}}{(f_{L1} + f_{L2})^2}[&f_{L1}^2 + f_{L1}f_{L2}\exp(2ika) \\ &+ f_{L2}f_{L1}\exp(-2ika) + f_{L2}^2], \end{aligned} \quad (28)$$

where i is the imaginary unit.

5. Evaluation with real data

The analytic and the semianalytic model are both evaluated with real data from the field testing of lidar-assisted control. Here, a scanning lidar system from the University of Stuttgart was installed at the National Wind Technology Center on the nacelle of the two-bladed Controls Advanced Research Turbine (CART2) with a rotor diameter of $D = 42.7$ m and a hub height of 36.8 m.

The signals necessary for this correlation study are obtained from lidar and turbine data; see Schlipf et al. (2012a) for more details. The rotor effective wind speed v_0 is estimated from measured turbine data by a non-linear estimator. For the lidar system, a circular trajectory with $n_{fp} = 6$ focus points in $n_{fd} = 5$ focus distances equally distributed between $1D$ and $2D$ diameters and a scan time of $T = 1.33$ s were used. Figure 2 shows both signals from the considered 5-min period together with the wind speed measured with the anemometer on the nacelle. The lidar provides a preview signal that coincides with the wind speed estimate from the turbine for low frequencies. The anemometer measures a lower wind speed because of its position behind the rotor, which extracts energy from the wind. With the comparison to the analytic and semianalytic models, it can be confirmed that the lack of correlation for high
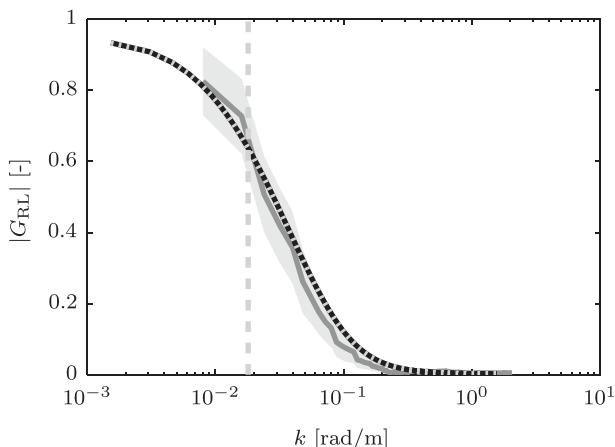
FIG. 3. Transfer function of the nacelle anemometer and the CART2: analytic model (black), coinciding semianalytic model (light gray, dotted), measured (dark gray), and $\pm\sigma$ confidence bounds (light gray shading). Maximum wavenumber $\hat{k} = 0.018\,\mathrm{rad\,m^{-1}}$ (dashed).
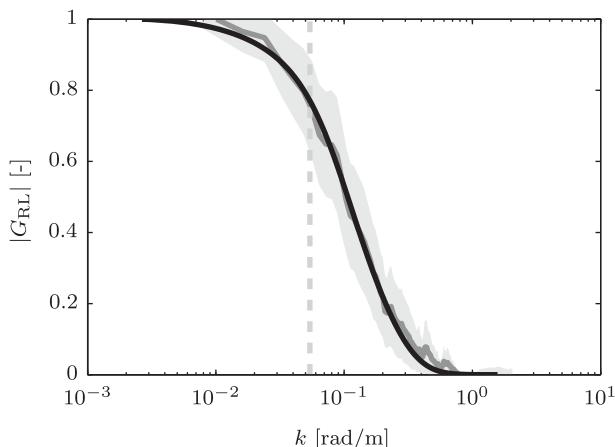

FIG. 4. Transfer function of the scanning lidar system and the CART2: analytic (black), measured (dark gray), and $\pm\sigma$ confidence bounds (light gray shading). Maximum wavenumber $\hat{k} = 0.054\,\mathrm{rad\,m^{-1}}$ (dashed).

frequencies is caused by the combination of the effects described in section 4.

a. Evaluation of the analytic model

The analytic model cannot be evaluated with a real lidar system because wind evolution and volume measurement cannot be neglected. Therefore, the anemometer signal is compared to rotor effective wind speed. Figure 3 shows that the transfer function based on (10) and (12) fits to the data. Confidence bounds are calculated based on Bendat and Piersol (1971). Furthermore, the transfer function based on the semianalytic model (16) with $n = 357$ equally over the rotor area distributed points with 2-m separation is close to the one of the fully analytic model. The separation distance is chosen as a compromise between accuracy and computational effort.

b. Evaluation of the semianalytic model

To model the volume of the pulsed lidar system, a Gaussian shape weighting function $f_L(a)$ with a full width at half maximum (FWHM) of $W = 30\,\mathrm{m}$ is used, following the considerations of Lindelöw (2008) and Banakh and Smalikho (1997):

$$
\begin{aligned}
f_L(a) &= \frac{\exp\left(-4\ln2\,\dfrac{a^2}{W^2}\right)}{\displaystyle\int_{-\infty}^{\infty} \exp\left(-4\ln2\,\dfrac{a^2}{W^2}\right)da} \\
&= \frac{2\ln2\exp\left(-4\ln2\,\dfrac{a^2}{W^2}\right)}{W\sqrt{\ln2\pi}}.
\end{aligned} \tag{29}
$$

The weighting function is discretized at $n_{\mathrm{wp}} = 5$ equally distributed points with a distance of 10 m. In Simley et al. (2013) the volume averaging is considered as a source of error when comparing to a single-point measurement and beneficial when comparing to a blade effective wind speed. The weighting function also is beneficial for the determination of the rotor effective wind speed, because more information is collected over the rotor disk. Furthermore, the dimensionless longitudinal decay parameter $\alpha = 0.4$ is roughly estimated with a staring lidar system measuring from a wind turbine based on Schlipf et al. (2010b). For the model v_0 is obtained by $n = 357$ equally over the rotor area distributed points with 2-m separation. The modeled $v_{0\mathrm{L}}$ is calculated by a sum of $3n_{\mathrm{fp}}n_{\mathrm{fd}}n_{\mathrm{wp}} = 450$ signals of the u, v, and w wind components.

Figure 4 shows good agreement with the data. Based on this model, a filter depending on the mean wind speed $\overline{u}$ was fitted with a maximum coherent wavenumber of $\hat{k} = 0.06\,\mathrm{rad\,m^{-1}}$. Similar agreement was achieved in the

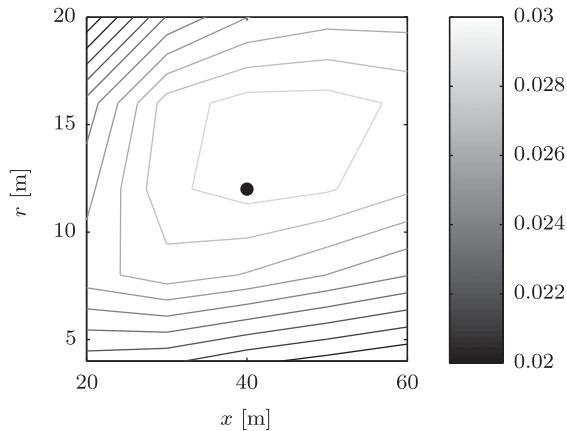FIG. 5. Scope of a lidar system with three beams.

FIG. 6. Maximum coherent wavenumber $\hat{k}$ (rad m^{-1}) of a lidar system with three beams at different distances and radii on a turbine with $D = 40$ m. The optimum is marked with a dot.

field testing with a commercial lidar system and the three-bladed CART (CART3; Scholbrock et al. 2013).

6. Lidar system optimization

The proposed model can be used to optimize the configuration or the scanning pattern of a lidar system. As an example the model is used to determine the optimum correlation of a lidar system with three independent beams on a turbine with $D = 40$ m. For this purpose, the measurement distance x and the scan radius r are varied in a brute force optimization (see Fig. 5). The value of the wavenumber $\hat{k}$ at -3 dB below the steady value of the transfer function is shown in Fig. 6. An optimum value ($\hat{k} = 0.03$ rad m^{-1}) can be found at $x = 40$ m and $r = 12$ m.

7. Conclusions and outlook

This work presents a model to estimate the correlation of the rotor effective wind speed between a lidar system and a wind turbine, considering different rotor diameters, spatial averaging, different scanning patterns, and wind evolution, which—in combination—are responsible for the level of correlation. The derived model is modular, and all changes can be applied in a straightforward manner that makes it usable to optimize the configuration and scan pattern of lidar systems. The model is evaluated with data from a field testing campaign, where the results were used to rate lidar measurements and to design the filter that is the crucial part of the successfully tested feedforward collective pitch controller. In future work the model will be extended to model the correlation of rotor effective shears for lidar-assisted cyclic pitch control.

REFERENCES

Banakh, V. A., and I. N. Smalikho, 1997: Estimation of the turbulence energy dissipation rate from the pulsed Doppler lidar data. *Atmos. Oceanic Opt.,* **10,** 957–965.

Bendat, J. S., and A. G. Piersol, 1971: *Random Data: Analysis and Measurement Procedures.* John Wiley & Sons, 407 pp.

Bossanyi, E., 2012: Un-freezing the turbulence: Improved wind field modelling for investigating lidar-assisted wind turbine control. *Proc. European Wind Energy Association Annual Event,* Copenhagen, Denmark, EWEA. [Available online at http://proceedings.ewea.org/annual2012/allfiles2/912_EWEA2012 presentation.pdf.]

Dunne, F., D. Schlipf, L. Y. Pao, A. D. Wright, B. Jonkman, N. Kelley, and E. Simley, 2012: Comparison of two independent lidar-based pitch control designs. *Proc. 50th AIAA Aerospace Sciences Meeting Including the New Horizons Forum and Aerospace Exposition,* Nashville, TN, AIAA, AIAA 2012-1151.

Henriksen, L. C., 2011: Model predictive control of wind turbines. Ph.D. thesis, Technical University of Denmark, 132 pp.

IEC, 2005: Wind turbines—Part 1: Design requirements. IEC 61400-1, 92 pp.

Jonkman, B. J., and M. L. Buhl, 2007: TurbSim user's guide. NREL Tech. Rep. NREL/TP-500-41136, 35 pp.

Kapp, S., and M. Kühn, 2012: A five-parameter wind field estimation method based on spherical upwind lidar measurements. *Proc. Conf. on the Science of Making Torque from Wind,* Oldenburg, Germany, EAWE, in press.

Koerber, A., and R. King, 2011: Nonlinear model predictive control for wind turbines. *Proc. European Wind Energy Association 2011 Annual Event,* Brussels, Belgium, EWEA, 6 pp. [Available online at http://proceedings.ewea.org/annual2011/allfiles2/1105_EWEA2011presentation.pdf.]

Kragh, K. A., M. H. Hansen, and T. Mikkelsen, 2013: Precision and shortcomings of yaw error estimation using spinner-based light detection and ranging. *Wind Energy,* **16,** 353–366, doi:10.1002/we.1492.

Kristensen, L., 1979: On longitudinal spectral coherence. *Bound.-Layer Meteor.,* **16,** 145–153.

Laks, J., L. Y. Pao, A. Wright, N. Kelley, and B. Jonkman, 2010: Blade pitch control with preview wind measurements. *Proc. 48th AIAA Aerospace Sciences Meeting Including the New Horizons Forum and Aerospace Exposition,* Orlando, FL, AIAA, AIAA 2010-251.

——, E. Simley, and L. Pao, 2013: Spectral models for evaluating the effect of wind evolution on wind turbine preview control. *Proc. American Control Conf.,* Washington, DC, IEEE CCS and AACC, TuB18.5.

Lindelöw, P., 2008: Fiber based coherent lidars for remote wind sensing. Ph.D. thesis, Technical University of Denmark, 163 pp.

Pielke, R. A., and H. A. Panofsky, 1970: Turbulence characteristics along several towers. *Bound.-Layer Meteor.,* **1,** 115–130.

Schlipf, D., and M. Kühn, 2008: Prospects of a collective pitch control by means of predictive disturbance compensation assisted by wind speed measurements. *Proc. Ninth German Wind Energy Conf.,* Bremen, Germany, German Wind Energy Institute, 4 pp. [Available online at http://elib.uni-stuttgart.de/opus/volltexte/2013/8433/.]

——, J. J. Trujillo, V. Basterra, and M. Kühn, 2009: Development of a wind turbine LIDAR simulator. *Proc. European Wind Energy Conf.,* Marseille, France, EWEA, 6 pp. [Available online at http://proceedings.ewea.org/ewec2009/allfiles2/655_EWEC2009presentation.pdf.]

——, T. Fischer, C. E. Carcangiu, M. Rossetti, and E. Bossanyi, 2010a: Load analysis of look-ahead collective pitch control using lidar. *Proc. 10th German Wind Energy Conf.,* Bremen, Germany, German Wind Energy Institute, 4 pp. [Available online at http://elib.uni-stuttgart.de/opus/volltexte/2013/8432/.]

——, and Coauthors, 2010b: Testing of frozen turbulence hypothesis for wind turbine applications with a scanning lidar system. *Proc. 15th Int. Symp. for the Advancement of Boundary Layer Remote Sensing,* Paris, France, IPSL, O-WIN/02.

——, S. Kapp, J. Anger, O. Bischoff, M. Hofsäß, A. Rettenmeier, and M. Kühn, 2011: Prospects of optimization of energy production by lidar assisted control of wind turbines. *Proc. European Wind Energy Association 2011 Annual Event,* Brussels, Belgium, EWEA, 10 pp. [Available online at http://proceedings.ewea.org/annual2011/allfiles2/914_EWEA2011presentation.pdf.]

——, P. Fleming, F. Haizmann, A. Scholbrock, M. Hofsäß, A. Wright, and P. W. Cheng, 2012a: Field testing of feedforward collective pitch control on the CART2 using a nacelle-based lidar scanner. *Proc. Conf. on the Science of Making Torque from Wind,* Oldenburg, Germany, EAWE, 3-8.

——, A. Rettenmeier, M. Hofsäß, M. Courtney, and P. W. Cheng, 2012b: Model based wind vector field reconstruction from lidar data. *Proc. 11th German Wind Energy Conf.,* Bremen, Germany, German Wind Energy Institute. [Available online at http://elib.uni-stuttgart.de/opus/volltexte/2013/8431/.]

——, P. Fleming, S. Kapp, A. Scholbrock, F. Haizmann, F. Belen, A. Wright, and P. W. Cheng, 2013a: Direct speed control using lidar and turbine data. *Proc. American Control Conf.,* Washington, DC, IEEE CCS and AACC, MoC18.1.

——, D. J. Schlipf, and M. Kühn, 2013b: Nonlinear model predictive control of wind turbines using lidar. *Wind Energy,* doi:10.1002/we.1533, in press.

Scholbrock, A., P. Fleming, L. Fingersh, A. Wright, D. Schlipf, F. Haizmann, and F. Belen, 2013: Field testing lidar based feed-forward controls on the NREL controls advanced research turbine. *Proc. 51st AIAA Aerospace Sciences Meeting Including the New Horizons Forum and Aerospace Exposition,* Grapevine, TX, AIAA, 2013-0818.

Simley, E., L. Y. Pao, N. Kelley, B. Jonkman, and R. Frehlich, 2012: Lidar wind speed measurements of evolving wind fields. *Proc. 50th AIAA Aerospace Sciences Meeting Including the New Horizons Forum and Aerospace Exposition,* Nashville, TN, AIAA, AIAA-2012-0656 .

——, ——, R. Frehlich, B. Jonkman, and N. Kelley, 2013: Analysis of light detection and ranging wind speed measurements for wind turbine control. *Wind Energy,* doi:10.1002/we.1584, in press.

Taylor, G., 1938: The spectrum of turbulence. *Proc. Roy. Soc. London,* **132A,** 476–490.